REPORT DOCUMENTATION PAGE

Form Approved
OMB No. 0704-0188

Public reporting burden for this collection of information is estimated to average 1 hour per response, including the time for reviewing instructions, searching existing data sources, gathering and maintaining the data needed, and completing and reviewing this collection of information. Send comments regarding this burden estimate or any other aspect of this collection of information, including suggestions for reducing this burden to Department of Defense, Washington Headquarters Services, Directorate for Information Operations and Reports (0704-0188), 1215 Jefferson Davis Highway, Suite 1204, Arlington, VA 22202-4302. Respondents should be aware that notwithstanding any other provision of law, no person shall be subject to any penalty for failing to comply with a collection of information if it does not display a currently valid OMB control number. **PLEASE DO NOT RETURN YOUR FORM TO THE ABOVE ADDRESS.**

1. REPORT DATE *(DD-MM-YYYY)*	2. REPORT TYPE	3. DATES COVERED *(From - To)*
February 2012	Journal Article	

4. TITLE AND SUBTITLE

Erosion Measurements in a Diverging Cusped-Field Thruster (Pre Print)

5a. CONTRACT NUMBER

5b. GRANT NUMBER

5c. PROGRAM ELEMENT NUMBER

6. AUTHOR(S)
Stephen R. Gildea, Taylor S. Matlock, Manuel Martinez-Sanchez and William A. Hargus, Jr.

5d. PROJECT NUMBER

5f. WORK UNIT NUMBER
Q0AZ

7. PERFORMING ORGANIZATION NAME(S) AND ADDRESS(ES)

Air Force Research Laboratory (AFMC)
AFRL/RZSS
1 Ara Drive
Edwards AFB CA 93524-7013

8. PERFORMING ORGANIZATION REPORT NUMBER

9. SPONSORING / MONITORING AGENCY NAME(S) AND ADDRESS(ES)

Air Force Research Laboratory (AFMC)
AFRL/RZS
5 Pollux Drive
Edwards AFB CA 93524-7048

10. SPONSOR/MONITOR'S ACRONYM(S)

11. SPONSOR/MONITOR'S NUMBER(S)
AFRL-RZ-ED-JA-2012-040

12. DISTRIBUTION / AVAILABILITY STATEMENT

Approved for public release; distribution unlimited (PA #12113).

13. SUPPLEMENTARY NOTES
For publication in Journal of Propulsion & Power.

14. ABSTRACT

Results from a long duration test of a cusped-field plasma thruster operating at an anode power of 165 W are presented and discussed. Profile measurements of the boron nitride insulator were performed before and after the 204 h test, enabling the quantification of average erosion rates over a large portion of the interior. Unlike most Hall thrusters, the lifetime is not limited by erosion near the exit plane, due to the positioning of magnetic circuit elements. Additionally, the maximum erosion rate is found to be lower than rates measured in low-power Hall thrusters by at least 50%. The lifetime of this laboratory prototype is estimated at 1220 h based on the time needed to erode through the insulator in one of the ring-cusps. Therefore, fortifying cusps with additional or a more durable material would increase the lifetime of future designs. A summary of long duration tests and erosion measurements in Hall thrusters is also provided. A concurrent analysis of deposition within the thruster shows the accumulation of a conductive and ferromagnetic material between cusps. Finally, estimates of electron temperature and ion loss widths near the wall are obtained based on measured distributions of erosion in each cusp. During the tests discussed here, the thruster operated in the "high-current" mode, characterized by strongly oscillatory anode currents. Erosion rates upstream of the exit cusp may be lower in the "low-current" mode, where anode current oscillation amplitudes are smaller by two orders of magnitude.

15. SUBJECT TERMS

16. SECURITY CLASSIFICATION OF:			17. LIMITATION OF ABSTRACT	18. NUMBER OF PAGES	19a. NAME OF RESPONSIBLE PERSON
					Dr. William R. Hargus, Jr.
a. REPORT	b. ABSTRACT	c. THIS PAGE	SAR	21	19b. TELEPHONE NUMBER *(include area code)*
Unclassified	**Unclassified**	**Unclassified**			N/A

Erosion Measurements in a Low-Power, Cusped-Field Plasma Thruster

Stephen R. Gildea,* Taylor S. Matlock,† and Manuel Martínez-Sánchez‡
Massachusetts Institute of Technology, Cambridge, MA, 02139, USA

and

William A. Hargus, Jr.§
Air Force Research Laboratory, Edwards Air Force Base, CA 93524, USA¶

Abstract: Results from a long duration test of a cusped-field plasma thruster operating at an anode power of 165 W are presented and discussed. Profile measurements of the boron nitride insulator were performed before and after the 204 h test, enabling the quantification of average erosion rates over a large portion of the interior. Unlike most Hall thrusters, the lifetime is not limited by erosion near the exit plane, due to the positioning of magnetic circuit elements. Additionally, the maximum erosion rate is found to be lower than rates measured in low-power Hall thrusters by at least 50%. The lifetime of this laboratory prototype is estimated at 1220 h based on the time needed to erode through the insulator in one of the ring-cusps. Therefore, fortifying cusps with additional or a more durable material would increase the lifetime of future designs. A summary of long duration tests and erosion measurements in Hall thrusters is also provided.

A concurrent analysis of deposition within the thruster shows the accumulation of a conductive and ferromagnetic material between cusps. Finally, estimates of electron temperature and ion loss widths near the wall are obtained based on measured distributions of erosion in each cusp. During the tests discussed here, the thruster operated in the "high-current" mode, characterized by strongly oscillatory anode currents. Erosion rates upstream of the exit cusp may be lower in the "low-current" mode, where anode current oscillation amplitudes are smaller by two orders of magnitude.

Nomenclature

ξ	= Erosion rate
S_ξ	= Volumetric erosion coefficient
$\Delta\phi_s$	= Sheath potential drop
r_e, r_i	= Electron and ion Larmor radii
j_{iw}	= Ion current density at wall
T_e, T_i	= Electron and ion temperatures

*Ph.D. Candidate, Aeronautics & Astronautics, sgildea@mit.edu
†Ph.D. Candidate, Aeronautics & Astronautics, tmatlock@mit.edu
‡Professor, Aeronautics & Astronautics, mmart@mit.edu
§Research Scientist, Space Propulsion Branch, william.hargus@edwards.af.mil
¶Distribution A: Approved for public release; distribution unlimited.

I. Introduction

Interest in small satellites continues to grow as newly demonstrated capabilities lead to more ambitious mission objectives. In addition to cost savings associated with lighter payloads, more launch opportunities are available for systems that can be accommodated by multiple launch vehicles. With this flexibility, the use of small satellites allows more independent objectives to be met for a given cost, increasing accessibility to space. Advantages are offset somewhat by more stringent constraints on propulsion systems, diminishing or eliminating the maneuverability of small satellites in orbit. Satellites piggybacking with larger payloads are then forced to operate exclusively in the insertion orbit, and concerns about the accumulation of orbital debris may limit the number of launch opportunities for small satellites in the future. These difficulties could be mitigated by extending the benefits of electric propulsion to this class of satellites, increasing their utility to research, industrial, and governmental communities.

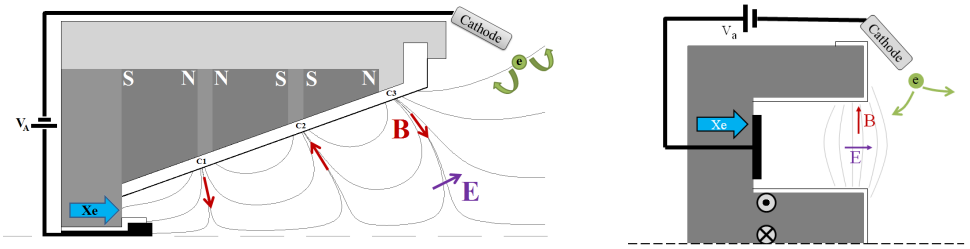

(a) DCFT schematic with representative magnetic field lines overlayed. Note the existence of discrete magnetic cells, bounded by separatrix surfaces.

(b) Schematic of a Hall thruster.

Figure 1. Schematics representing cusped-field and Hall thrusters.

The study of more efficient and durable low-power Hall thruster concepts is an active area of research in many countries[1–5]. This is motivated by the operational heritage of Hall thrusters in space, with proven efficiencies and lifetimes greater than 50% and 7000 h, respectively[6,7]. Figure 1(b) illustrates the standard configuration of a Hall thruster, characterized by an annular discharge chamber, anode, and neutral injector. Typically, a noble gas such as xenon is injected into the thruster near the anode while a cathode located downstream emits low energy electrons. The anode is biased positive relative to cathode potential, initiating ionization of the gas via collisions with electrons accelerating upstream. Electromagnets are used to establish a mostly radial magnetic field with a maximum of several hundred gauss near the exit plane, confining electrons in a closed Hall drift perpendicular to the applied fields. The much heavier ions are not confined by the magnetic field, and are instead accelerated away by the electric field, providing thrust. The electric field in the region of electron confinement is needed to balance the magnetic force on the azimuthal electron current. Without the magnetic field to hinder the axial mobility of electrons, they would effectively shield the plasma bulk from the applied DC electric field, resulting in poor performance.

Scaling Hall thruster designs to low powers while maintaining high efficiencies has proven challenging, especially below 200 W, as shown in Table 1. Alternatively, plasma thrusters with markedly different magnetic topologies and field strengths have also been examined. The cylindrical Hall thruster (CHT) concept has been studied at low to moderate power levels, but recent efforts have focused on low-power applications[8,9]. The magnetic field strength is larger than in Hall thrusters, with maximum values of ≈ 1 kG. Near the exit, magnetic field lines are mostly radial, converging axially further upstream along the centerline. This topology is similar to the end-Hall thruster[10], though the field is much stronger in the CHT. Also, the anode remains annular in CHT designs, to give electrons a longer cross-field path to the anode. More detailed aspects of the design depend on whether the magnetic field is provided by electric currents or permanent magnets, or how the magnetic poles are arranged[11]. The anode efficiency of the thruster varies between 13-38% over a power range of 60-220 W, depending on the thruster design, cathode keeper current, and which parameters are included in the efficiency calculation[9]. Although no direct results quantifying erosion rates or lifetime for the CHT have been reported, a smaller surface-area-to-volume ratio is often cited as the reason a CHT would be more durable than a Hall thruster operating at an equivalent anode power.

The diverging cusped-field thruster (DCFT) is another low-power alternative presently being investigated. As shown in Figure 1(a), permanent ring-magnets of alternating polarity downstream of a magnetic pole piece give rise to several regions containing convergent magnetic field lines, referred to as cusps. In addition to the three ring-cusps, point-cusps are established on the thruster axis to either side of each ring-cusp - at the anode and downstream of C3, for instance. The ring-cusps are referred to in their order proceeding downstream from the anode: the first cusp (C1),

Table 1. Survey of low-power Hall thrusters for which lifetime and performance data were found in the literature. The primary reference is listed with the thruster designation, while additional sources are indicated where appropriate. The listed anode powers correspond to operating conditions used during the long duration tests, while representative anode efficiencies are listed in cases where efficiency measurements at the tested anode power were not available. In some cases, the insulator may be penetrated by erosion - termed a "soft-failure"[12] - though the lifetime of the thruster is predicted to exceed this time. It is necessary to make this distinction because some authors provide useful thruster lifetimes in excess of the soft-failure time. A more complete summary of Hall thruster erosion measurements is provided in Table 4.

Thruster Designation	Anode Power [W]	Anode Efficiency	Soft-Failure Time [h]	Predicted Lifetime [h]
SPT-50[13]	320	47%	>2,500$^{\times}$	-
KM-45[14]	310	40-50%[1]	3,500-4,000	-
KM-32[2]	200	30-40%	2,000-3,000	3,000*
BHT-200[15]	200	43.5%	1,287-1,519	>1,700
HT-100[16]	175	25%[4]	300[17]	1,500[17]**
SPT-30[18]	150	26%[19]	600*	-
SPT-20M[20]	<100	$\leq$38%[5]	594-910	4,000

- Indicates data not found in reviewed literature.

$\times$ Details of method leading to prediction not given.

$*$ Center pole is measurably eroded before hour 500 of testing.

$**$ Predicted lifetime pertains to 100 W anode power, rather than the tested 175 W condition.

second cusp (C2), and third cusp (C3). Unlike CHTs and Hall thrusters, the anode is cylindrical, located on the thruster axis with magnetic field lines mostly normal to its surface. Rather than trying to manage cross-field electron diffusion, electron mobility near the anode is impeded by a magnetic mirroring effect. Field strengths along the axis exceed 4 kG near the anode and 1 kG between C1 and C2, but decrease to zero where each ring-cusp separatrix intersects the centerline. Figure 14 provides calculated values of the total, parallel, and perpendicular components of the magnetic field along the wall, as well as a more detailed description and definition of separatrices.

The use of cusped magnetic fields in plasma thrusters did not begin with the DCFT concept. DC discharge ionization chambers in ion thrusters have long utilized magnetic cusps for plasma confinement[21]. However, a more direct precursor to the DCFT was the development of high efficiency multistage plasma (HEMP) thrusters by Kornfeld et al. in Germany[22]. HEMP thrusters also use permanent magnets to create magnetic cusps in the thruster chamber, and testing thus far has focused on power levels near 1.5 kW for applications on telecommunications satellites[23]. Engineering models of the HEMP 3050 have reported efficiencies of 45% with thrust and specific impulse values of 50 mN and 3000 s[22]. More provocative is the lifetime estimate, stated to be in excess of 18,000 h based on reported erosion rates that are smaller than those measured in comparable thrusters by a factor larger than 200[24].

The DCFT was developed to determine if cusped magnetic topologies could provide longer lifetimes to low-power thrusters with performance capabilities similar to Hall thrusters. Performance similar to the BHT-200, a commercially made and flight-proven thruster, was demonstrated in 2007 - with measured anode efficiencies between 40-45% at anode powers ranging from 185-275 W[25]. More recent measurements are in agreement with the initial results when uncertainties in each data set are considered[26]. Two operational modes have also been identified, termed the high-current (HC) and low-current (LC) modes. These names describe how, for a given anode flow rate, the anode current drops sharply when the anode voltage is increased above a threshold value. The change of modes is also accompanied by a change in the visual appearance of the plume, as shown in Figure 2. Later, the HC-mode was found to be accompanied by large-amplitude, low-frequency anode current oscillations, while those same oscillations were absent or greatly reduced in LC-mode[27,28]. Additional studies have included spectroscopy of the DCFT plasma[29], the effects of alternate magnetic topologies near the exit plane[30,31], and particle-in-cell simulations[32]. Ion velocity measurements clearly demonstrate that the location of the acceleration region is strongly correlated with the location of the C3 separatrix[33]. A similar design with a cylindrical chamber has also been investigated by the Stanford Plasma Physics Laboratory[34].

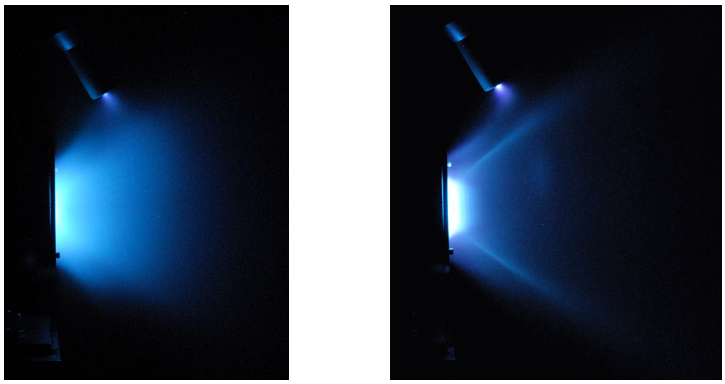

(a) DCF thruster operating in the high-current mode.

(b) DCF thruster operating in the low-current mode.

Figure 2. DCF Thruster operating in Chamber 1 at the Edwards AFB AFRL.

This paper presents erosion and performance measurements from a 204 h test of the DCF thruster. The vacuum system and data acquisition are described in Section II, along with the profilometer used to quantify erosion rates. Operational parameters are presented in Section III, followed by erosion measurements, and an analysis of surface deposition in Section IV. In Section V, the data are analyzed and discussed. Additionally, a review of previously reported lifetime and erosion data is used to put these results in context. Finally, from the size of the observed erosion features, estimates of electron temperature and ion loss widths in each cusp are presented.

II. Experimental Setup

The thruster was operated in Chamber 1 at the Space Propulsion Branch of the Air Force Research Laboratory (AFRL), located at Edwards Air Force Base (AFB). Chamber 1 is cylindrical, with a length of 4.1 m and a diameter of 2.4 m. The vacuum chamber is made of non-magnetic stainless steel, and the inner surface is covered by flexible sheets of graphite. Each end of the channel is protected by angled graphite panels to mitigate back sputtering, and the floor downstream of the thruster is covered by a graphite blanket for the same reason. The vacuum is established and maintained primarily by two 1.2 m gaseous helium two-stage cryogenic (15 K) pumps, with liquid nitrogen cooled (75 K) baffles. The total xenon pumping speed is 48,500 L/s. Pumping was supplemented by a turbomolecular pump, to affect gases such as hydrogen. Uncorrected chamber pressure was measured using a cold cathode gauge, calibrated for nitrogen, and reduced by a correction factor of 2.9 to account for xenon as the dominant gas constituent.

All thruster and cathode electrical power was provided by commercially available devices. The thruster anode and cathode keeper were each driven by a Sorensen DCS600-1.7E, while the cathode heater power was delivered by a Sorensen DLM 40-15. The anode was biased in reference to cathode potential, which was allowed to float with respect to chamber ground. Outputs from power supplies were calibrated using an Agilent 34410A Digital Multimeter. Purified xenon (99.995%) flow rates to the anode and cathode were set manually and delivered using a UNIT Instruments power supply and mass flow controllers. The cathode position, which has been shown to significantly affect thruster operation, was located identically to past studies[25]: 73 mm from the thruster axis of symmetry and 31 mm from the exit plane. During thruster operation, power supply voltages and currents, along with the cathode floating potential, were digitally recorded twice per second. Chamber pressure was recorded by hand until hour 60 of testing, at which point modifications to data acquisition software enabled automated recordings. After this point, pressure was recorded twice per second as well. A Busek BHC-1500 hollow cathode was used to initiate the discharge and neutralize the plume for all tests described herein.

Throughout all tests, the cathode heater current was fixed at 3.0 A to decrease the likelihood of the keeper voltage rising substantially and causing a shutdown during unsupervised operation. The keeper current was held constant at 0.5 A. Maintaining operation in LC-mode was not possible for more than ten minutes. As a result, the thruster operated in HC-mode at a single operating condition for nearly the entire test. An anode voltage of 300 V and mass flow rate of 8.5 $sccm$ were selected to avoid heating the permanent magnets above 300°C - the manufacturer listed maximum operating temperature[25]. The curie temperature for the magnets is higher, at 825°C. Unpublished tests with a thermocouple placed between the middle magnet and chamber insulation suggest an upper limit of 185-200 W to the

anode power to avoid overheating the magnets beyond 300°C. Additionally, laser-induced fluorescence velocimetry and thrust data are available at this operating condition from other campaigns[25,33].

The main purpose of this long duration test was to quantify erosion rates in the DCF thruster and evaluate the potential of this concept for extending available operational lifetimes of low-power plasma thrusters. Before and after the long duration test in Chamber 1, the profile of the insulating channel was measured using the Micromeasure system from Micro Photonics, Inc. This system consists of a STIL CHR150 chromatic confocal spectrometer, a CHR Contactless Optical Sensor, three linear stages and a power supply. The hardware and data acquisition are controlled by a desktop computer using a program called Surface Map. Specifications of the optical sensor and stepper motors are provided in Table 2, and a schematic of the profilometer is shown in Figure 3. The optical sensor was positioned at the angle allowing for the greatest signal strength a short distance upstream of C1. This was necessary because the signal intensity was not sufficient to allow measurements over a wide range incidence angles. Once a suitable orientation was found, the position of the sensor was secured and measured with the digital level described in Table 2. An additional requirement of the optical sensor position was line-of-sight accessibility to the reference region (described below), without having to change the sensor's orientation. This condition was imposed to avoid additional uncertainties related to the relative orientations of the optical sensor between scans.

Table 2. Specifications of the optical sensor, digital level, and stepper motors.

Optical Sensor		Flexbar PRO 360 Digital Level		Linear Stages	
Working Distance	66.9 *mm*	Accuracy, $\pm 10°$ from level/vertical	$\pm 0.1°$	Z-axis precision	0.01 μm
Measuring Range	10.0 *mm*	Maximum error, other angles	$\pm 0.2°$	X & Y axes precisions	0.1 μm
Lateral Resolution	25.5 μm	Range	360°		
Center Range Static Noise	556 *nm*				

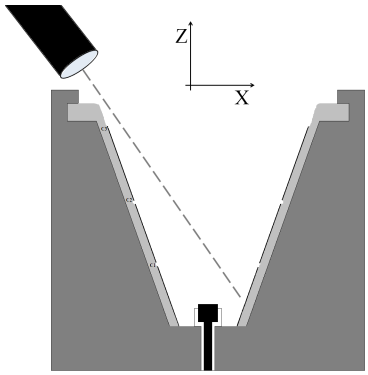

Figure 3. In this schematic, the optical sensor is illustrated measuring the surface position at a point upstream of C1.

Using the profilometer, the relative distances between two points in a scan can be determined to an accuracy better than 1 μm. However, quantifying erosion requires the determination of distances between points in different scans. This system is not configured to provide measurements while the thruster is under vacuum, so a method relating the coordinate systems of different scans was implemented.

A digital level was used along the X and Y axes to ensure that the exit plane of the thruster was parallel with the XY measurement plane. The zero-coordinate of the Y-axis for each scan was estimated as the average extrema location of parabolic fits to measured profiles of the distance from the optical sensor to the thruster surface. These centering data were obtained from sweeps of the Y-coordinate at constant values of X. Then, the detailed topology of a small feature carved out of a protected part of the thruster was measured with the profilometer. Scans of the reference feature were made before and after operating the thruster. The coordinate systems of the erosion scans were then related to one another through the coordinate transformations necessary to match the two reference scans. Figure 15 shows the "before" scan matched to the "after" scan of the reference feature, to within $\pm 10 \mu m$. The matching scheme could be improved if the coordinate transformation were obtained through the constrained minimization of an error function. However, in this case, plots similar to Figure 15 were inspected visually to select the coordinate transformation that most closely matched the contours. The quoted uncertainty from the technique is the smallest change in each

coordinate that caused a noticeable difference in the similarity of the two scans.

After testing was complete and post-test profiles were measured, a sample of the surface was taken for analysis using Energy Dispersive X-ray Spectroscopy (EDS). The sample consists of wall material removed from the entire interior of the surface, so no definitive statements about the distribution of materials on the surface can made. Also, some of the material removed was clearly magnetized, gathering in the cusps of the thruster.

III. Long Duration Test

The thruster and cathode ran at a single operating condition for almost the entirety of the test, given in Table 3. Throughout testing, the chamber pressure was 2-3 $\mu Torr$. The anode current is plotted in Figure 4(a), and remained between 0.53-0.56 A from 5.5 hours until the end of testing. Over the same interval, the floating cathode potential, relative to chamber ground, began at -16 V and slowly increased to -12 V. However, the cathode keeper voltage remained between 11-13 V with the aid of a constant 3.0 A heater current. The repeated drops in anode current correspond with intentional thruster shutdowns to allow for thrust stand calibration and subsequent measurements. These measurements are not described in detail because the thrust stand was not configured properly before testing. After analyzing the data, the standard deviations of measured anode efficiencies were larger than $\pm 10\%$. The average values of thrust, specific impulse, and anode efficiency were significantly and consistently lower than other DCFT performance measurements[26,35]. Standard deviations near or exceeding 50% of average values were seen in most cases. The average thrust values also decreased as the thruster operated, though any trends in the average were within uncertainty margins. The poor quality of these data does not warrant further discussion at this point.

Table 3. Thruster and cathode operating condition during the long duration test.

Anode Flow	8.5 sccm
Anode Voltage	300 V
Cathode Flow	1.5 sccm
Keeper Current	0.5 A
Heater Current	3.0 A

The anode current took on a wider range of values over the first 5.5 hours of testing. The thruster ignited near the 2.5 h mark after cathode conditioning. Operation in LC-mode was attempted during the first 10 minutes of testing. The anode current crept up with time in conjunction with the sporadic onset of current pulses - a conspicuous precursor to the transition from LC to HC-mode. After this was observed, the decision was made to operate in HC-mode, and the operating parameters were set to the values listed in Table 3. From here, the current rose above 600 mA, very similar to the anode current measured during initial performance measurements performed at Busek in 2007[25]. Then, as seen in Figure 4(b), during a period slightly less than half an hour, the current dropped below 500 mA, and then rose gently and leveled off at 510 mA. All operating conditions were held constant over this time, and the thruster was left unattended between hours 3.5 and 60. During this time, the anode current rose from 510 mA to 550 mA just after hour 5, where it remained above 538 mA until hour 55.38, when it dropped suddenly again to 532 mA. After this, the anode current varied smoothly until the end of the test. However, the onset of very low frequency anode current oscillations is evident starting between hours 90 and 100. These had a period of several minutes and their amplitude increased with time until testing concluded. As shown in Figure 4(c), the amplitude near hour 200 was 10-20 mA. Changes in the cathode potential, also shown in Figure 4(c), coincide with fluctuations in the anode current, though they are negatively correlated.

The visual appearance of the thruster is documented in Figure 5. Before any testing, the BN cone is clean and white, as seen in Figure 5(a). Contrastingly, Figure 5(b) shows the insulator after 65-70 h of operation, but prior to the experiments described in this report. The walls are dark and black, except for white rings visible in each cusp. Finally, after an additional 204 h of firing, the accumulation of more deposition on the walls is visible in Figure 5(c). Parts of the wall appear lighter than surrounding areas, and with shades of grey or white. The cause of this coloration is unknown, but an elemental analysis of the deposition is discussed in Section IV.

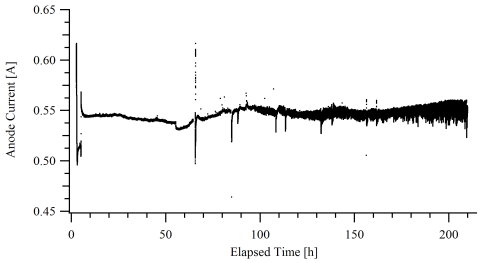

(a) Anode current during the entire test.

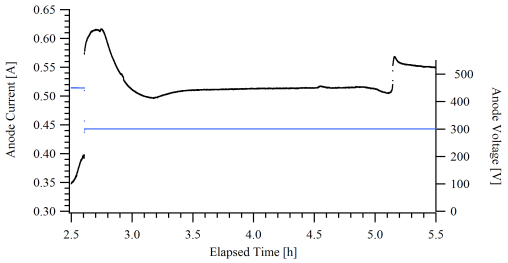

(b) Anode current and voltage during the first several hours of operation. The current (voltage) scale is on the left (right) axis.

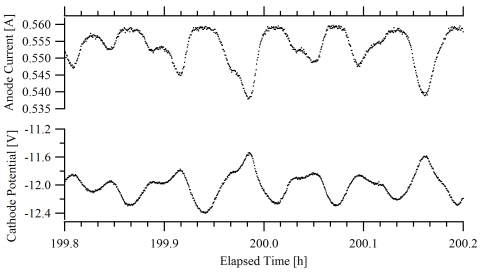

(c) Anode current and cathode potential near hour 200. Axial increments in time are 1 *min*. Very low frequency oscillations were first noticed near hour 100 of testing, and increased in amplitude as the test continued.

Figure 4. Anode current during testing.

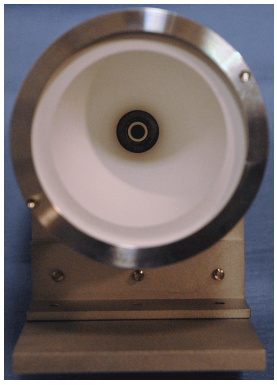

(a) The thruster before operation.

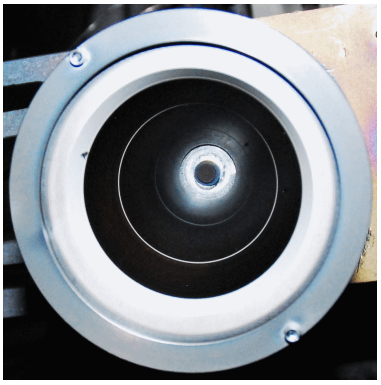

(b) The thruster after 65-70 *h* of operation, but before the start of the long duration test.

(c) The thruster after 204 *h* of operation at the conditions given in Table 3, for a total run time of 269-274 *h*. The aluminum cap holding the cone in place has been removed in preparation for profilometry.

Figure 5. Photographs of the HP BN insulator at different stages of its operational history. The thruster is oriented with the cathode to the left in Figure 5(b), and above the thruster in Figure 5(c).

IV. Erosion Quantification & Deposition Analysis

The profile of the insulating HP BN cone was measured before and after the long duration test. An overview of the measurements is given in Figure 6, showing the locations of maximum erosion relative to the permanent magnets and insulator. Each scan sampled the surface height along a 0.5 *mm* wide strip, with a 25 μm step size. The data points plotted in Figures 6 and 7 represent the average coordinates of data points along the width of the strip. The offset of points from the center of the strip was included in calculating the average radial coordinate. The systematic error introduced to this average by the curvature of the measurement surface is less than 1 μm, much less than the errors due to coordinate system matching. Erosion is limited to the immediate vicinity of the cusp locations in C1 and C2. Closer to the exit plane, erosion begins near C3 and continues toward the exit plane. Detailed plots of the measured profiles in the cusp regions are given in Figure 7. The reason for less resolution on the downstream side of the erosion feature visible in Figure 7(b) is due to the slope of the surface relative to the incident beam of light. The dependence of measurement resolution on the relative orientations of the surface and light beam is illustrated in Figure 8(a).

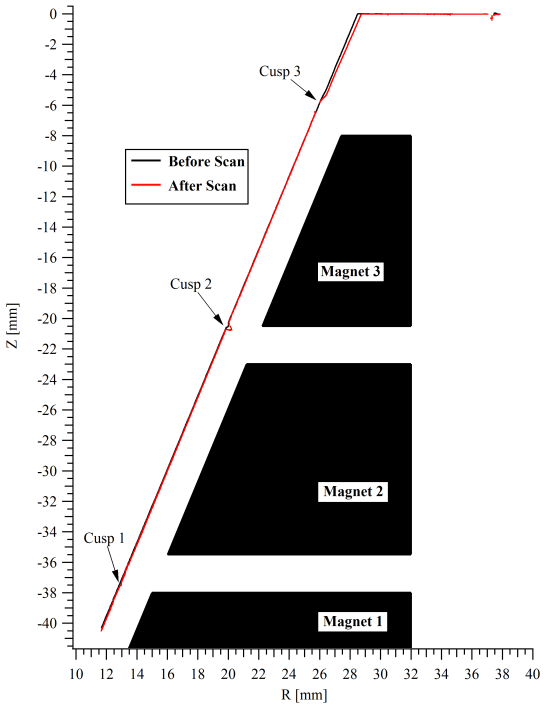

Figure 6. Profilometer scans, before and after 204 h of operation at the operating condition given in Table 3. Magnets are numbered in their order downstream of the anode. The exit plane of the thruster corresponds to $z = 0$. Measurements were limited to just upstream of C1, due to the angle of the incident beam of light and to more specular reflection of incident light closer to the anode.

From these two profiles, average erosion rates are calculated based on the distances between them, perpendicular to the original cone surface - which has a 22.5° half-angle with respect to the centerline. Referring to Figure 8(b), this is done by fitting a line perpendicular to the nominal wall angle through a point in the "after" scan, referred to as point "A". Next, the point of intersection between this line and a segment joining two points in the "before" scan is found, referred to as point "B". The distance between A and B (d_{AB}) is taken as the eroded distance corresponding to point B. The results are shown in Figures 9 and 10, where the erosion rate is plotted in terms of the radial coordinates of interpolated points from the "before" scan. Comparing Figures 10(b) and 7(b), this explains why the plotted erosion rate is double valued in areas where the "before" profile is sufficiently curved from preexisting erosion. It also explains why the shapes of the cusps do not match those visible in Figure 7. The slope of erosion data between cusps in Figure 9 is due to a 0.25° misalignment, very close to the precision of the level used to position the thruster for measurements. The alignment error is smallest where the alignment was made, and increases closer to C1. The effect of the error is to *overestimate* the maximum erosion rate of the thruster by about 0.15 $\mu m/h$. Aside from this systematic error, the statistical uncertainty of the eroded depths is estimated at $\pm 20 \mu m$. Therefore, the uncertainties in the maximum erosion rate and estimated lifetime are ± 0.1 $\mu m/h$ and ± 60 h, respectively.

The peak erosion rate is in C2, rather than at the exit plane as observed in Hall thrusters, with a maximum average

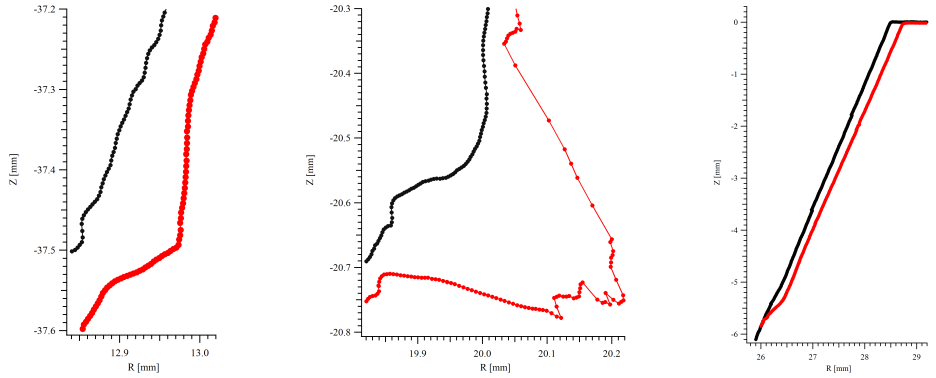

(a) Cusp 1 detail. (b) Cusp 2 detail. (c) Cusp 3 detail.

Figure 7. As in Figure 6, the "before" ("after") profile is shown in black (red). Note the different scales in each figure.

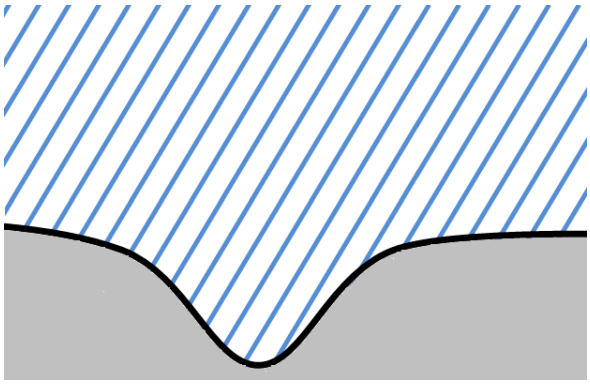

(a) The dependence of measurement resolution on surface slope relative to the incidence angle of the beam. As the beam and surface become more parallel, the resolution of the measurement for a given step size deteriorates. If the surface slope goes past parallel with the beam, a portion of the surface will be inaccessible for measurement unless the beam angle is changed.

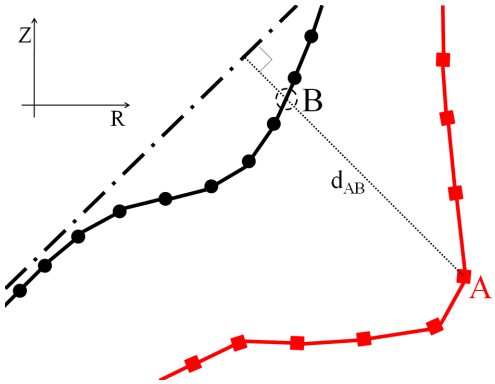

(b) The eroded distance is determined from the distance between points A and B. Point A is measured in the "after" scan, while point B is interpolated from two points in the "before" scan.

Figure 8. These illustrations are meant to demonstrate how measurement resolution is affected by surface slope, and how the eroded distance is calculated.

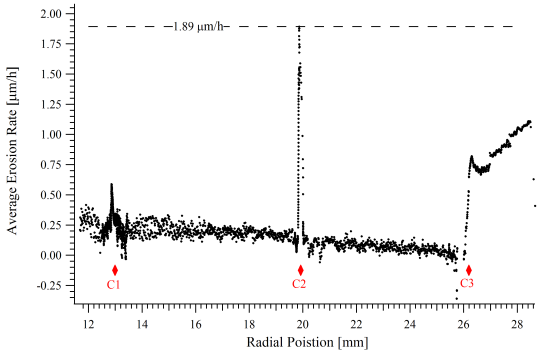

Figure 9. Average erosion rate during the 204 hours of operation. The locations of the cusps along the wall are indicated by the red diamonds. The DCFT lifetime is therefore limited to 1200 h by erosion in the second cusp. The statistical uncertainties of the maximum erosion rate and estimated lifetime are $\pm 0.1\ \mu m/h$ and $\pm 60\ h$, respectively.

value of 1.9 $\mu m/h$. The first and second ring-cusps coincide with regions of increased erosion, while C3 is roughly where erosion at the exit begins in the downstream direction along the thruster wall. Erosion rates increase toward the exit, but never exceed the erosion rate measured in the second cusp. The initial thickness of the insulating cone is 2.5 *mm* in the radial direction, allowing for an effective insulation lifetime of 1220 *h*. This lifetime is calculated assuming a constant erosion rate in the second cusp. Many Hall thrusters are predicted to continue operating after the insulating ceramic is unable to completely shield the magnetic circuit - see Table 4. This is appropriately referred to as a "soft failure"[12] in situations where a satellite and thruster can continue to function within specifications after the insulator has been compromised. An extensive comparison of beginning-of-life (BOL) erosion rates and thruster lifetimes determined from measurements in Hall thrusters is provided in Table 4. A distinction is made between the predicted lifetime of a thruster and the time at which soft failure is reported or predicted to occur.

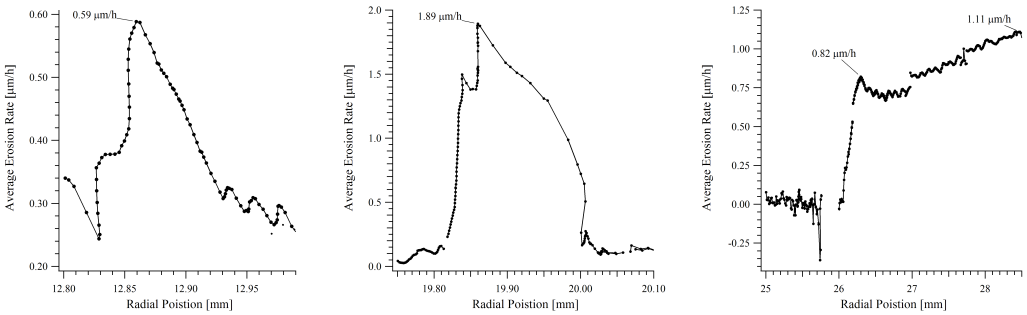

(a) Cusp 1 average erosion rates. (b) Cusp 2 average erosion rates. (c) Cusp 3 average erosion rates.

Figure 10. Average erosion rate measurements in each ring cusp. The coordinate on the horizontal axis is the radial coordinate of an interpolated point in the "before" scan. Note the different scales in each of these figures.

Deposition on the cone surface during operation was also significant. Figure 11 shows photographs of different areas of the cone surface after the test was completed. These photos should be compared to Figure 5(b) to observe the difference in the appearance before and after testing. The coloring of the deposition is lightest near the porous 316 stainless steel diffuser behind the anode up until the first ring-cusp. Downstream of C1, the deposition is mostly darker, with the exceptions of some areas that are lighter grey or white in between cusps. The direct source of these previously unseen patterns is not known, but they exhibit some symmetry with respect to the cathode location. A sample of the deposition was scrapped off with a teflon coated spatula and analyzed using EDS. Localized samples were not taken, preventing the examination of compositional variation between different areas of the chamber. A sample of deposited materials on an external surface was also analyzed.

The composition of the internal deposition contained copper, constituents of 316 stainless steel and additives commonly used to lower the work function of tungsten in hollow cathode emitters. The exterior sample was composed entirely of copper, tin and other components common to copper alloys. The portion of the thrust stand visible in Figure 12 is made of copper to allow for more efficient active cooling using an exterior cold water supply, and is likely the source of copper identified in both deposition samples. The large amount of iron on the interior is likely sputtered from the annular porous stainless steel disc located upstream of the anode. The diffuser disc is visible in Figures 5 and 11. The source of lighter deposition on the upper and side surfaces is not known, but the symmetry of the pattern suggests that it originates from the cathode.

V. Discussion & Analysis of Erosion Measurements

These measurements show erosion localized in the immediate vicinity of the cusps and toward the exit plane. In Figures 9 and 10(c), the erosion rate downstream of C3 increases because ions, on average, do not experience the main potential drop until they encounter the last separatrix in the chamber[33]. Aside from the local peak in erosion rate at C3, the increase in erosion toward the exit is also observed at the inner and outer poles of Hall thrusters. Measurements of Hall thruster erosion are referenced in Table 4. Unlike Hall thrusters, however, erosion near the exit in the DCF thruster takes place entirely downstream of the magnetic circuit, visualized in Figure 6. Therefore, erosion near the exit plane is not the limiting factor in the operational lifetime of the DCF thruster.

For this implementation of the cusped-field concept, the maximum average erosion rate was measured as 1.9 $\mu m/h$ and occurs in the second ring cusp. As erosion in this location continues, the magnetic circuit will be exposed. By

(a) Photo of the left half cone surface, facing the anode.

(b) Photo of the right half cone surface, facing the anode.

Figure 11. Photos of the DCFT insulator after testing was completed. Eroded regions are evident as white rings in each cusp. The uneven, but somewhat symmetrical, pattern of deposition is also visible. The location of the cathode is above the thruster for the orientations shown here.

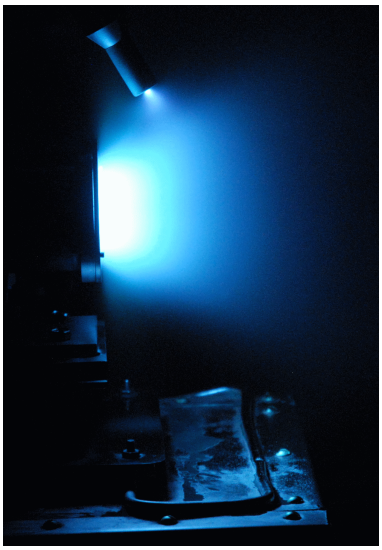

Figure 12. The plume, overexposed in this photograph, illuminates the thrust stand.

assuming a constant erosion rate along the thinnest path through the insulating cone, a lifetime estimate of 1220 h is justified for this design. Referring again to Table 4, for thrusters operating near 200 W or less, only the DCF and BHT-200 thrusters have the reported capability of operating past 1000 h without exposing components of their magnetic circuit. The DCF insulator is predicted to fail 70-300 h before the BHT-200. These measurements also indicate that the maximum erosion rate in the DCF thruster is lower by a factor of two or more than the rates reported for thrusters operating at 325 W or less.

The ion loss width and electron temperature in each cusp can be estimated based on the full width at half maximum (FWHM) of the erosion profiles. Assigning a Gaussian distribution centered about the separatrix at the wall for the erosion rate (ξ) and ion current density (j_{iw}), Eq. 1 provides a relationship between the FWHM (δ) of each variable. Knorr and Willis have shown that plasma leak widths through cusps with no parallel electric field are proportional to the geometric mean of the electron and ion Larmor radii, often referred to as the hybrid radius[58]. This is consistent with observations that the leak width scales as $(m_i)^{1/4}$ [59]. The cusp leak width, given in Eq. 2, is defined as the FWHM of the potential well (δ_ϕ) at the loss point. Empirically, the value of the constant A in Eq. 2 is about two. Potential wells in ring-cusps of the DCF thruster have been measured with flush mounted wall probes and are reproduced in kinetic simulations as well[32,60].

$$\xi = j_{iw}\, S_\xi(E,\theta) = j_{iw}\, S_E\, S_\theta \tag{1}$$

$$\delta_\phi = 2A\sqrt{r_e r_i} \tag{2}$$

The FWHM of j_{iw} (δ_j) can be approximated as δ_ϕ because the ions are electrostatically confined by the electric field arising due to the stronger confinement of electrons in the magnetic field. For any pair of ion and electron temperatures, the hybrid Larmor radius is calculated using the thermal speeds $\sqrt{\frac{kT_s}{m_s}}$ for ions and electrons. The pre-sheath structure along a separatrix is very similar to the standard case in the absence of a magnetic field[61], setting the maximum sheath potential drop as a function of the electron temperature. Secondary electron emission and space charge saturation are accounted for using fits for the yield dependence on T_e from Goebel and Katz (p. 348-349,353)[21] and a reduced sheath voltage[62]. The energies of ions entering the sheath are assumed to be negligibly small compared to the sheath potential, allowing the distribution of incident ion energies to be calculated directly from the potential distribution set by T_e. With the ion energies (E), the distribution of S_ξ for normal impacts is found using Eq. 3, provided by Yim[63]. The fit is based on molecular dynamics simulations of HBC grade BN sputtered by xenon ions at a surface temperature of 423 K. The normalization convention forces $S_\theta \approx 0.6$ for ions normal to the surface, an additional assumption.

$$S_E = 0.06\left[1-\left(\frac{18.26}{E}\right)^{2/3}\right]\left[1-\frac{18.26}{E}\right]^2, \quad [mm^3/C] \tag{3}$$

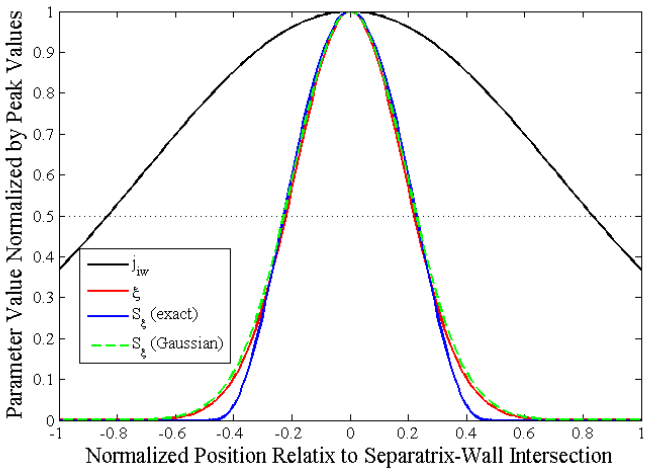

Figure 13. A comparison of the distributions of j_{iw}, ξ, and S_ξ used in the estimates for C1 shown in Table 5.

The system is solved iteratively by finding the value of T_e near the wall for which the FWHM of the right side of Eq. 1 matches the measured values. For these estimates, an ion temperature of 0.05 eV is chosen. The assumed

Table 4. A compilation of erosion data and lifetime estimates available for SPT-Hall effect thrusters. The THALES HEMP 3050 and MIT DCFT are also included. The reference cited with the thruster designation is the primary source for the data presented in the corresponding row. Additional references are provided when the desired information was found in a different source. Multiple entries in a cell correspond to different values reported in separate references. The reviewed literature was restricted to papers written in English, with one exception [20].

Thruster Designation	Predicted Lifetime [h]	Single Thruster Test Duration [h]	Magnetic Pole/Circuit Exposure Time [h]	Tested Anode Power [kW]	Max. "BOL" Erosion Rate [$\mu m/h$]	Insulator Material†	Operational Chamber Pressure (Xe) [$\mu Torr$]
T-220 [36]	>4,800	1,028	4,800*	10	12	-	31-32
BPT-4000 [37]	>20,000-40,000	10,400	20,000-40,000*	4.5,(1-4.5)	-	BN [38]	10-25
SPT-140 [39]	>6,300	>1,000	-	4.5	13.2	borosil [40]	16-32, 77
NASA-103M.XL [41]	>15,000× [42]	5,000	>15,000	3.1, 3.5	-	BN [42]	-
HEMP 3050 [24]	>18,750	250, 800 [43]	>18,750*	1.8, 1.4 [43]	.04	BN	-
NASA-120M [44]	-	200	-	1.65	9.0	HP BN	-
PPS®1350-G [45]	>10,530‡	10,530	<10,530	1.5	10.4 [46], 6	-	110 [46]
SPT-100 [47]	>9,000‡,×, [6,48]	7,515	<7,000 [49]	1.35	10.1 [50]	borosil [51]	<50, 14.5 [52], 5 [53]
EM-900 [54]	3,000	500	3,000*	.864	11.7, 11.9	BN-05 & BGP	30-50
UT-1 kW HET [55]	-	-	-	.690	≈9.0	BN	42
SPT-70 [6]	≥3,000×,‡	-	-	.660	3.6 [56]	borosil, BGP-10 [56]	-, <60 [56]
BHT-600 [15]	>932	932	-	.615	≈3.6 [57]	HBC BN	5.3 [57]
SPT-50 [13]	≥2,500×	825	-	.320	-	borosil	50-100
KM-45 [14]	3,500-4,000	1,020	3,500-4,000*	.310	4.1	-	10-20
KM-32 [2]	3,000‡	500	2,000-3,000*	.200	5.2	HP BN	23, 12
BHT-200 [15]	>1,700‡	>1,700	1,287-1,519	.200	≈3.8 [57]	HBC BN	2.2 [57]
HT-100 [16]	1,500×,‡,§ [17]	445	300 [17]	.175	9	60/40:BN/SiO_2 [4]	7.5
MIT DCFT	>1,220	204	1,220*	.165	1.9	HP BN	2-3
SPT-30 [18]	600×	-	-	.150	-	borosil	-
SPT-20M [20]	4,000‡	1,000	594-910	<.100	-	alumina [5] w/ additive	24 [5]

- Indicates data not found in reviewed literature.

* Indicates an extrapolation from measured erosion profiles, not an experimental demonstration

† A material grade is specified where possible. If the grade is not specified, it was not found in the reviewed literature.

‡ Indicates that the magnetic circuit is exposed at or before the listed number of hours. This is sometimes referred to as "soft failure" [12].

× Details of lifetime test leading to prediction were not found in reviewed literature.

§ Predicted lifetime pertains to 100 W anode power, rather than the tested 175 W condition.

Gaussian distributions of erosion rate and j_{iw} allow the right side to be evaluated because we have assumed $\delta_j = \delta_\phi$, where δ_ϕ is evaluated using Eq. 2. The estimated values of the maximum ion current density in each cusp are in Table 5. From this analysis, the ion loss widths in the cusps are about twice as wide as erosion regions, where δ_ξ is the measured FWHM of the erosion rate. Furthermore, the average electron temperatures in C2 and C3 are comparable. Predictions of j_{iw} are highly sensitive to the chosen value of T_i. For instance, using $T_i = 0.5\ eV$, rather than $0.05\ eV$ as before, causes the predicted value of j_{iw} to increase an order of magnitude. The sensitivities of predicted values for T_e, $\Delta\phi_s$, δ_ϕ and sheath saturation are weaker, with δ_ϕ increasing by only 40% for this example. A direct comparison to previous measurements is not warranted because the operating conditions are different in each case[32,60]. The secondary electron yield (SEY) was not permitted to exceed 0.983, and the sheath is considered saturated when the SEY attains this value.

Figure 13 is an example of the solution of this model corresponding to the first cusp. From this, it would be reasonable to assign a Gaussian distribution to S_ξ as well, providing the more approximate relationship between lengths scales shown in Eq. 4 - where δ_S is the FWHM of S_ξ. This provides a much simpler mathematical explanation of why $\delta_\xi < \delta_j$. For instance, setting $\delta_S = \delta_j$ provides $\delta_j = \sqrt{2}\delta_\xi$. The precise factor is given by the energy dependance of S_ξ and the mathematical form of the spatial distributions (e.g. Gaussian, Lorentzian). Therefore, the width of the erosion feature must be smaller than the ion current density loss width.

Admittedly, the erosion profile at C3 is not as clearly peaked as in C1 and C2, though a half peak is apparent in Figure 10(c) between $R = 26 - 26.5\ mm$. The half-width of that distribution was doubled to allow C3 to be included in the estimates presented here. Estimates of S_ξ were unable to account for possibly elevated wall temperatures in cusps due to a lack of measurements and incomplete data regarding temperature effects on erosion rates for BN. These effects may be significant, as Yim shows S_ξ doubling over a temperature range from 420-1050 K for simulations of xenon sputtering BN with an incidence energy of 50 eV[63]. The analysis also assumes equality between electron temperatures parallel and perpendicular to magnetic field lines.

$$\frac{1}{\delta_\xi^2} \approx \frac{1}{\delta_j^2} + \frac{1}{\delta_S^2} \tag{4}$$

Table 5. Estimates of ion loss width and electron temperature near the wall, based on measured widths of erosion features in each cusp.

		C1	C2	C3
δ_ξ	$[mm]$	.15	.25	.61
B	$[G]$	4560	4420	1590
T_e	$[eV]$	6.7	24	21
$\Delta\phi_s$	$[V]$	29	29	25
Sheath Saturated		N	Y	Y
$S(\Delta\phi_s, 0) \times 10^{-3}$	$[mm^3/C]$	2.3	4.6	3.1
j_{iw}	$[A/m^2]$	71	115	74
δ_ϕ	$[mm]$	.35	.50	1.3

VI. Conclusions

The DCF thruster was subjected to a long duration test to measure average erosion rates of the insulating ceramic. The thruster operated consistently in HC-mode throughout, with the average anode current remaining within a range of 30 mA for the last 98.5% of the 204 h test. Very low frequency oscillations in the anode current were observed, increasing in amplitude as the test continued. The deposition of conductive, ferromagnetic material on the BN insulator was also identified. This motivates avoiding further use of stainless steel in the interior of laboratory thrusters.

Profilometry in each cusp was completed, as well as in between cusps. Erosion features in the cusps and downstream of C3 firmly establish the locations of wall losses in cusped-field thrusters. The peak average erosion rate was 1.9 $\mu m/h$, measured in the second cusp. This is lower than any limiting erosion rate reported in the reviewed Hall thruster literature, even amongst thrusters with anode powers less than 200 W. A lifetime estimate based on this erosion rate is 1220 h. The design examined here is a laboratory prototype, originally intended for exploratory testing of the cusped-field thruster concept.

The observation of higher erosion in C2 than in C3 was unexpected and may offer insight into important differences between the HC and LC-modes. The anode current in HC-mode is characterized by ~ 3 kHz oscillations with magnitudes several times larger than the average value. Therefore, the electron temperature estimates shown in Table 5 must be interpreted as time averages over the oscillation period. High-speed digital videos show that the HC-mode instability is accompanied by an increase in luminosity from the plasma upstream of the exit plane[28]. One possible interpretation of these observations is that an ionization avalanche is initiated throughout the thruster, consuming a large fraction of the available neutrals. Ions created during this burst of ionization are more easily lost to the second cusp than ions created near the exit because of the potential valley present in the bulk within ring-cusps[32,60,61]. This particular cusp occupies the largest volume in the interior of the thruster chamber, as shown in Figure 1(a). Rather than moderate, steady amounts of ionization that must be present in the LC-mode, the emerging view of the HC-mode is one of near complete ionization of the neutral population as some instability is triggered, leading to spikes in the anode current. The time between bursts is set by the neutral replenishment time scale. As such, second cusp erosion in the LC-mode, where ionization is steady and presumably localized near the third cusp, is expected to be lower than in the HC-mode mode. Confirming this hypothesis, and the extent to which the erosion is lessened, will require further experimental and numerical investigation. Quantifying erosion in the low-current mode will be an important goal of continued studies involving the DCFT.

Acknowledgements

The authors thank P. Adkison, J. Blakely, M. Holmes, M. Nakles, and G. Reed of the Space Propulsion Branch at the Edwards AFB AFRL for their assistance in completing these experiments. P. Boisvert of the MIT Electron Microscopy Shared Experimental Facility is also acknowledged for his assistance in the acquisition of data for the deposited material analysis. R. Sullivan is thanked for her insights regarding the possible effects of redeposited iron on internal thruster surfaces. Research on cusped-field thrusters at the Massachusetts Institute of Technology Space Propulsion Laboratory is funded through the Air Force Office of Scientific Research. S. Gildea acknowledges the Science Mathematics & Research for Transformation (SMART) Scholarship for providing financial support of his academic work and the opportunity to work at the Space Propulsion Branch.

Appendix

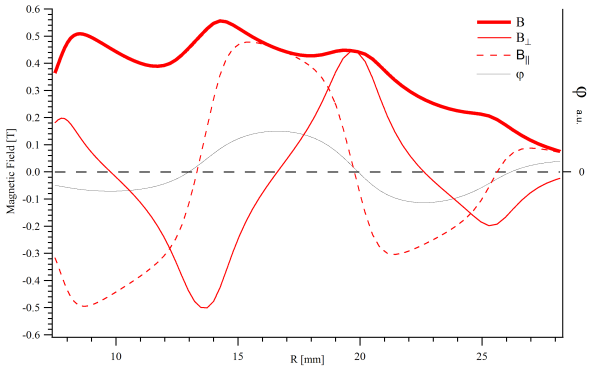

Figure 14. The parallel and perpendicular components of the magnetic field along the thruster wall are plotted, as well as the magnitude of the field and value of the magnetic stream function (φ). This magnetic stream function is proportional to the product of the radial coordinate and the azimuthal component of the magnetic vector potential, so lines of constant φ represent magnetic field lines. The dividing surfaces between magnetic cells are called separatrices, and are defined as those surfaces whose stream function value is zero. Thus, the rigorous locations of the magnetic cusps along the wall are where the stream function value is zero. The values plotted here were calculated using the MAXWELL SV software package. Field strength measurements along the thruster axis validate the simulated results [25].

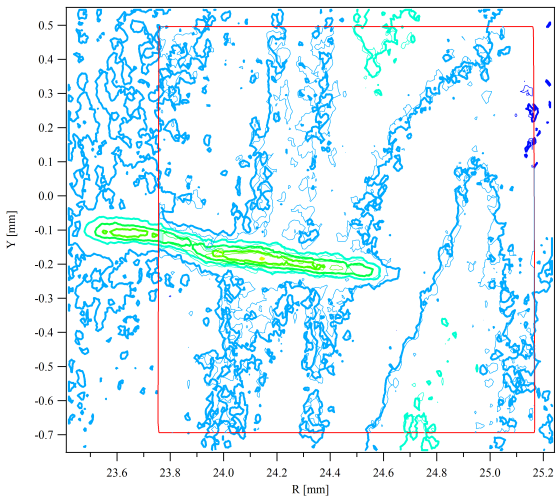

Figure 15. Contour plots of height for two scans of area surrounding the reference feature. The coordinate transformation used to provide this match was used to relate the coordinate systems of the "before" and "after" scans to one another. Identically colored lines represent equivalent surface heights, and appear in divisions of $10\mu m$. The thicker set of lines represents data from the "after" reference scan, while the thin lines show the measured heights from the "before" reference scan. The red square outlines the domain of data for the "before" reference scan. The uncertainty in alignment resulting from this approach is estimated to be $10\mu m$. Note that the scales of the two axes are not equal.

References

[1] Gorshkov, O., Belikov, M., Muravlev, V., Shagayda, A., Shanbhogue, K., Premkumar, S., Nandalan, V., and Jayaraman, M., "The GEOSAT Electrical Propulsion Subsystem Based on the KM-45 HET," *Acta Astronautica*, Vol. 63, No. 1-4, 2008, pp. 367 – 378.

[2] Belikov, M. B., Gorshkov, O. A., Dyshlyuk, E. N., Lovtzov, A. S., and Shagayda, A. A., "Development of Low-Power Hall Thruster with Lifetime up to 3000 Hours," 30th *International Electric Propulsion Conference*, Florence, IT, September 2007, IEPC-2007-129.

[3] Hargus, Jr., W. and Nakles, M. R., "Ion Velocity Measurements Within the Acceleration Channel of a Low-Power Hall Thruster," *Plasma Science, IEEE Transactions on*, Vol. 36, No. 5, October 2008, pp. 1989 –1997.

[4] Saverdi, M., Signori, M., and Biagioni, L., "Experimental Characterization of the HT-100 Hall Thruster in Twin Engine Cluster Configuration," 30th *International Electric Propulsion Conference*, Florence, IT, September 2007, IEPC-2007-320.

[5] Loyan, A. V. and Maksymenko, T. A., "Performance Investigation of SPT-20M Low Power Hall Effect Thruster," 30th *International Electric Propulsion Conference*, Florence, Italy, September 2007, IEPC-2007-100.

[6] Kozubskii, K., Murashko, V., Rylov, Y., Trifonov, Y., Khodnenko, V., Kim, V., Popov, G., and Obukhov, V., "Stationary Plasma Thrusters Operate in Space," *Plasma Physics Reports*, Vol. 29, 2003, pp. 251–266.

[7] Martínez-Sánchez, M. and Pollard, J. E., "Spacecraft Electric Propulsion - An Overview," *Journal of Propulsion and Power*, Vol. 14, No. 5, 1998, pp. 688–699.

[8] Raitses, Y. and Fisch, N. J., "Parametric Investigations of a Nonconventional Hall Thruster," *Physics of Plasmas*, May 2001.

[9] Diamant, K. D., Pollard, J. E., Raitses, Y., and Fisch, N. J., "Ion Velocity Measurements Within the Acceleration Channel of a Low-Power Hall Thruster," *Plasma Science, IEEE Transactions on*, Vol. 38, No. 4, April 2010, pp. 1052–1057.

[10] Kaufman, H. R., Robinson, R. S., and Seddon, R. I., "End-Hall Ion Source," *Journal of Vacuum Science and Technology A*, Vol. 5, No. 4, 1987, pp. 2081–2084.

[11] Polzin, K. A., Raitses, Y., Gayoso, J. C., and Fisch, N. J., "Comparisons in Performance of Electromagnet and Permanent-Magnet Cylindrical Hall-Effect Thrusters," 46th *Joint Propulsion Conference & Exhibit*, Nashville, TN, July 2010, AIAA-2010-6695.

[12] Hofer, R. R., Mikellides, I. G., Katz, I., and Goebel, D. M., "BPT-4000 Hall Thruster Discharge Chamber Erosion Model Comparison with Qualification Life Test Data," 30th *International Electric Propulsion Conference*, Florence, IT, September 2007, IEPC-2007-267.

[13] Arkhipov, B., Bober, A., Day, M., Gnizdor, R., Kozubsky, K., and Maslennikov, N., "Extending the Range of SPT Operation - Development Status of 300 and 4500 W Thruster," 32nd *Joint Propulsion Conference & Exhibit*, Lake Buena Vista, FL, July 1996, AIAA-1996-2708.

[14] Belikov, M. B., Gorshkov, O. A., Muravlev, V. A., Rizakhanov, R. N., Shagayda, A. A., and Vasin, A. I., "Qualification of Hall Thruster for Small Spacecraft Applications," *The Tenth International Workshop on Combustion and Propulsion*, Lerici, IT, September 2003, paper 19.

[15] Cheng, S. Y. and Martínez-Sánchez, M., "Hybrid Particle-in-Cell Erosion Modeling of Two Hall Thrusters," *Journal of Propulsion and Power*, Vol. 24, No. 5, 2008, pp. 987–998.

[16] Misuri, T., Tavoni, S., and Andrenucci, M., "Monte Carlo Erosion Model for HT-100 Lifetime Prediction," *ESA/3AF Space Propulsion Conference*, San Sebastian, ES, May 2010.

[17] Rossetti, P. and Andrenucci, M., "HT-100 Development Status," 31st *International Electric Propulsion Conference*, Ann Arbor, MI, September 2009, IEPC-2009-126.

[18] Kim, V., Kozlov, V., Lazurenko, A., Popov, G., Skrylnikov, A., Clauss, C., Day, M., and Sancovic, J., "Development and Characterization of Small SPT," 34th *Joint Propulsion Conference & Exhibit*, Cleveland, OH, July 1998, AIAA-1998-3335.

[19] Jacobson, D. T. and Jankovsky, R. S., "Test Results of a 200 W Class Hall Thruster," 34th *Joint Propulsion Conference & Exhibit*, Cleveland, OH, July 1998, AIAA-1998-3792.

[20] Loyan, A. V., Maksymenko, T. A., Rybalov, O. P., and Podgorny, V. A., "The Investigations of Erosion of Discharge Chamber of Low Power Stationary Plasma Thruster During Long-Continued Lifetime Test," АВИАЦИОННО-КОСМИЧЕСКАЯ ТЕХНИКА И ТЕХНОПОГИЯ, Vol. 65, No. 8, 2009, pp. 121–124.

[21] Goebel, D. M. and Katz, I., *Fundamentals of Electric Propulsion*, John Wiley and Sons, Inc., 2008.

[22] Kornfeld, G., Koch, N., and Harmann, H.-P., "Physics and Evolution of HEMP-Thrusters," 30th *International Electric Propulsion Conference*, Florence, Italy, September 2007, IEPC-2007-108.

[23] Harmann, H.-P., Koch, N., and Kornfeld, G., "Low Complexity and Low Cost Electric Propulsion System for Telecom Satellites Based on HEMP Thruster Assembly," 30th *International Electric Propulsion Conference*, Florence, IT, September 2007, IEPC-2007-114.

[24] Kornfeld, G., Harmann, H.-P., and Koch, N., "Status and Limited Life Test Results of the Cylindrical HEMP 3050 Thruster," 41st *Joint Propulsion Conference & Exhibit*, Tucson, Arizona, July 2005, AIAA-2005-4223.

[25] Courtney, D. G., "Development and Characterization of a Diverging Cusped Field Thruster and a Lanthanum Hexaboride Hollow Cathode," S.M. Thesis, Massachusetts Institute of Technology, Cambridge, MA, June 2008.

[26] Daspit, R., Lozano, P., and Martínez-Sánchez, M., "Characterization and Optimization of a Diverging Cusped Field Thruster with a Calibrated Horizontal Accelerometer," 48th *Joint Propulsion Conference & Exhibit*, San Diego, CA, July 2011, AIAA-2011-6069.

[27] Gildea, S., Martínez-Sánchez, M., Nakles, M., and Hargus, Jr., W. A., "Experimentally Characterizing the Plume of a Divergent Cusped-Field Thruster," 31st *International Electric Propulsion Conference*, Ann Arbor, MI, September 2009, IEPC-2009-259.

[28] Gildea, S. R., Matlock, T. S., Lozano, P., and Martínez-Sánchez, M., "Low-Frequency Oscillations in the Diverging Cusped-Field Thruster," 46th *Joint Propulsion Conference & Exhibit*, Nashville, TN, July 2010, AIAA-2010-7014.

[29] Matlock, T. et al., "Spectroscopic and Electrostatic Investigation of the Diverging Cusped-Field Thruster," 45th *Joint Propulsion Conference & Exhibit*, Denver, Co, August 2009, AIAA-2009-4813.

[30] Matlock, T., Gildea, S., Hu, F., Becker, N., Lozano, P., and Martínez-Sánchez, M., "Magnetic Field Effects on the Plume of a Diverging Cusped-Field Thruster," 46th *Joint Propulsion Conference & Exhibit*, Nashville, TN, July 2010, AIAA-2010-7104.

[31] Matlock, T. S., Hu, F., and Martínez-Sánchez, M., "Controlling Plume Divergence in a Cusped-Field Thruster," 32nd *International Electric Propulsion Conference*, Wiesbaden, DE, September 2011, IEPC-2011-178.

[32] Gildea, S. and Martínez-Sánchez, M., "Improvements in Divergent Cusped-Field Thruster Modeling," *ESA/A3F Space Propulsion Conference*, San Sebastián, ES, May 2010.

[33] MacDonald, N. A., Cappelli, M. A., Gildea, S. R., Martínez-Sánchez, M., and Hargus, Jr., W. A., "Laser-Induced Fluorescence Velocity Measurements of a Diverging Cusped Field Thruster," *Journal of Physics D: Applied Physics*, Vol. 44, 2011, pp. 295203.

[34] Young, C., Smith, A., and Cappelli, M., "Preliminary Characterization of a Diverging Cusped Field (DCF) Thruster," 31st *International Electric Propulsion Conference*, Ann Arbor, MI, September 2009, IEPC-2009-166.

[35] Courtney, D. G. and Martínez-Sánchez, M., "Diverging Cusped-Field Hall Thruster (DCHT)," 30th *International Electric Propulsion Conference*, Florence, Italy, September 2007, IEPC-2007-39.

[36] Mason, L. S., Jankovsky, R. S., and Manzella, D. H., "1000 Hours Testing on a 10 Kilowatt Hall Effect Thruster," 37th *Joint Propulsion Conference & Exhibit*, Salt Lake City, UT, July 2001, AIAA-2001-3773.

[37] de Grys, K., Mathers, A., Welander, B., and Khayms, V., "Demonstration of 10,400 Hours of Operation on a 4.5 kW Qualification Model Hall Thruster," 46*th* *Joint Propulsion Conference & Exhibit*, Nashville, TN, July 2010, AIAA-2010-6698.

[38] de Grys, K., Welander, B., Dimicco, J., Wenzel, S., Kay, B., Khayms, V., and Paisley, J., "4.5 kW Hall Thruster System Qualification Status," 41*st* *Joint Propulsion Conference & Exhibit*, Tucson, AZ, July 2005, AIAA-2005-3682.

[39] Gnizdor, R., Kozubsky, K., Maslennikov, N., Murashko, V., Pridannikov, S., and Kim, V., "Performance and Qualification Status of Multimode Stationary Plasma Thruster SPT-140," 26*th* *International Electric Propulsion Conference*, Kitakyushu, JP, October 1999, IEPC-1999-090.

[40] Stuckey, P., Clauss, C., Day, M., Murashko, V., Maslennikov, N., Kozubsky, K., Gnizdor, R., Arhipov, B., Popov, G., Kim, V., Kozlov, V., and Grdlichko, D., "SPT-140 High Performance Hall System (HPHS) Development," 34*th* *Joint Propulsion Conference & Exhibit*, Cleveland, OH, July 1998, AIAA-1998-4041.

[41] Kamhawi, H., Manzella, D., Pinero, L., Haag, T., and Huang, W., "In-Space Propulsion High Voltage Hall Accelerator Development Project Overview," 46*th* *Joint Propulsion Conference & Exhibit*, Nashville, TN, July 2010, AIAA-2010-6860.

[42] Kamhawi, H., Manzella, D., Pinero, L., Haag, T., Mathers, A., and Liles, H., "In-Space Propulsion High Voltage Hall Accelerator Development Project Overview," 45*th* *Joint Propulsion Conference & Exhibit*, Denver, Co, August 2009, AIAA-2009-5282.

[43] Koch, N., Harmann, H.-P., and Kornfeld, G., "Status of the THALES High Efficiency Multi Stage Plasma Thruster Development for HEMP-T 3050 and HEMP-T 30250," 30*th* *International Electric Propulsion Conference*, Florence, IT, September 2007, IEPC-2007-110.

[44] Peterson, P. Y. and Manzella, D. H., "Investigation of the Erosion Characteristics of a Laboratory Hall Thruster," 39*th* *Joint Propulsion Conference & Exhibit*, Huntsville, AL, July 2003, AIAA-2003-5005.

[45] Marchandise, F. R., Cornu, N., Darnon, F., and Estublier, D., "The PPS 1350-G Qualification Status 10500 h." 30*th* *International Electric Propulsion Conference*, Florence, IT, September 2007, IEPC-2007-164.

[46] Marchandise, F. R., Biron, J., Gambon, M., Cornu, N., Darnon, F., and Estublier, D., "The PPS® 1350 Qualification Demonstration 7500h on Ground, About 5000h in Flight," 29*th* *International Electric Propulsion Conference*, Princeton, NJ, October 2005, IEPC-2005-209.

[47] Gnizdor, R., Kozubsky, K., Koryakin, A., Maslennikov, N., Pridannikov, S., and Day, M., "SPT100 Life Test with Single Cathode up to Total Impulse Two Million Nsec," 34*th* *Joint Propulsion Conference & Exhibit*, Cleveland, OH, July 1998, AIAA-1998-3790.

[48] Kim, V., Popov, G., Arkhipov, B., Murashko, V., Gorshkov, O., Koroteyev, A., Garkusha, V., Semenkin, A., and Tverdokhlebov, S., "Electric Propulsion Activity in Russia," 27*th* *International Electric Propulsion Conference*, Pasadena, CA, October 2001, IEPC-2001-005.

[49] Arhipov, B. A., Bober, A. S., Gnizdor, R. Y., Kozubsky, K. N., Korakin, A. I., Maslennikov, N. A., and Pridannikov, S. Y., "The Results of 7000-Hour SPT-100 Life Testing," 24*th* *International Electric Propulsion Conference*, Moscow, RU, September 1995, IEPC-1995-39.

[50] Garner, C. E., Polk, J. E., Pless, L. C., Goodfellow, K. D., and Brophy, J. R., "Performance Evaluation and Life Testing of the SPT-100," 23*rd* *International Electric Propulsion Conference*, Seattle, WA, September 1993, IEPC-1993-091.

[51] Randolp, T., Kim, V., Kaufman, H., Kozubsky, K., Zhurin, V., and Day, M., "Facility Effects on Stationary Plasma Thruster Testing," 23*rd* *International Electric Propulsion Conference*, Seattle, WA, September 1993, IEPC-1993-097.

[52] Garner, C. E., Brophy, J. R., Polk, J. E., and Pless, L. C., "A 5,730-Hr Cyclic Endurance Test of The SPT-100," 31*st* *Joint Propulsion Conference & Exhibit*, San Diego, CA, July 1995, AIAA-1995-2667.

[53] Pencil, E. J., Randolph, T. R., and Manzella, D., "End-of-Life Stationary Plasma Thruster Far-Field Plume Characterization," 32nd *Joint Propulsion Conference & Exhibit*, Lake Buena Vista, FL, July 1996, AIAA-1996-2709.

[54] Abashkin, V. V., Gorshkov, O. A., Lovtsov, A. S., and Shagaida, A. A., "Analysis of Ceramic Erosion Characteristic in Hall-Effect Thruster with Higher Specific Impulse," 30th *International Electric Propulsion Conference*, Florence, Italy, September 2007, IEPC-2007-133.

[55] Cho, S., Yokota, S., Hara, K., Takahashi, D., Arakawa, Y., and Komurasaki, K., "Hall Thruster Channel Wall Erosion Rate Measurement Method Using Multilayer Coating Chip," 46th *Joint Propulsion Conference & Exhibit*, Nashville, TN, July 2010, AIAA-2010-6697.

[56] Khartov, S., Nadiradze, A., and Duchemin, O., "SPT Ceramic Isolator Surfaced Layer Composition Change with Lifetime," 28th *International Electric Propulsion Conference*, Toulouse, France, March 2003, IEPC-2003-059.

[57] Cheng, S. Y., "Modeling of Hall Thruster Lifetime and Erosion Mechanisms," Ph.D. Thesis, Massachusetts Institute of Technology, Cambridge, MA, 2007.

[58] Knorr, G. and Willis, D., "Leak Width of a Cusp-Confined Plasma," *Zeitschrift Naturforschung Teil A*, Vol. 37, 1982.

[59] Christensen, T., Hershkowitz, N., and Leung, K. N., "Mass Scaling of Permanent Magnet Line Cusp Plasma Leaks," *IEEE Transactions on Plasma Science*, Vol. PS-5, No. 1, March 1977.

[60] Matlock, T., Lozano, P., and Martínez-Sánchez, M., "Discharge Chamber Wall Flux Measurements in a Diverging Cusped-Field Thruster," *ESA/A3F Space Propulsion Conference*, San Sebastián, ES, May 2010.

[61] Martínez-Sánchez, M. and Ahedo, E., "Magnetic Mirror Effects on a Collisionless Plasma in a Convergent Geometry," *Physics of Plasmas*, Vol. 18, 2011, pp. 033509.

[62] Dunaevsky, A., Raitses, Y., and Fisch, N. J., "Secondary Electron Emission from Dielectric Materials of a Hall Thruster with Segmented Electrodes," *Phys. Plasmas*, Vol. 10, No. 6, 2003, pp. 2574–2577.

[63] Yim, J. T., "Computational Modeling of Hall Thruster Channel Wall Erosion," Ph.D. Thesis, The University of Michigan, Ann Arbor, MI, 2008.